Aalborg Universitet

Health indicator selection for state of health estimation of second-life lithium-ion batteries under extended ageing

Braco, Elisa; San Martin, Idoia; Sanchis, Pablo; Ursua, Alfredo; Stroe, Daniel-Ioan

Link to publication from Aalborg University

Research Papers

Health indicator selection for state of health estimation of second-life lithium-ion batteries under extended ageing

Elisa Braco [a,b], Idoia San Martin [a], Pablo Sanchis [a], Alfredo Ursúa [a,*], Daniel-Ioan Stroe [b]

[a] *Department of Electrical, Electronic and Communication Engineering, Institute of Smart Cities, Public University of Navarre (UPNA), Campus de Arrosadia, 31006 Pamplona, Spain*
[b] *Energy Department, Aalborg University, Pontoppidanstraede 101, 9220 Aalborg, Denmark*

ARTICLE INFO

ABSTRACT

Nowadays, the economic viability of second-life (SL) Li-ion batteries from electric vehicles is still uncertain. Degradation assessment optimization is key to reduce costs in SL market not only at the repurposing stage, but also during SL lifetime. As an indicator of the ageing condition of the batteries, state of health (SOH) is currently a major research topic, and its estimation has emerged as an alternative to traditional characterization tests. In an initial stage, all SOH estimation methods require the extraction of health indicators (HIs), which influence algorithm complexity and on-board implementation. Nevertheless, a literature gap has been identified in the assessment of HIs for reused Li-ion batteries. This contribution targets this issue by analysing 58 HIs obtained from incremental capacity analysis, partial charging, constant current and constant voltage stage, and internal resistance. Six Nissan Leaf SL modules were aged under extended cycling testing, covering a SOH range from 71.2 % to 24.4 %. Results show that the best HI at the repurposing stage was obtained through incremental capacity analysis, with 0.2 % of RMSE. During all SL use, partial charge is found to be the best method, with less than 2.0 % of RMSE. SOH is also estimated using the best HI and different algorithms. Linear regression is found to overcome more complex options with similar estimation accuracy and significantly lower computation times. Hence, the importance of analysing and selecting a good SL HI is highlighted, given that this made it possible to obtain accurate SOH estimation results with a simple algorithm.

1. Introduction

Environmental problems related to internal combustion vehicles, together with government actions and citizen awareness, have brought electric vehicles (EV) to the forefront of the automotive industry. This has a direct impact on the demand for Li-ion batteries for EVs, which reached 160 GWh in 2020 [1].

Due to usage, Li-ion batteries suffer from capacity and power fade, which may compromise their compliance with EV requirements. Therefore, automotive standards set 20 % to 30 % of capacity loss as a threshold value for the Li-ion batteries to be retired from EVs. Compared to traditional alternatives such as recycling, the reuse of Li-ion batteries in other applications leads to lifetime extension, thereby representing a beneficial solution from an economic and environmental point of view. Stationary applications, where energy density is not as crucial as in EVs, emerge as possible second-life (SL) usage scenarios. The potential of these SL batteries from EVs is such that the storage supply for stationary applications could exceed 200 GWh per year by 2030 [2].

However, the success of SL batteries from EVs is still uncertain today, given that this depends on their technical and economic viability. Even though the operation and durability of SL modules [3–5] and battery packs [6,7] from EVs has been experimentally assessed in recent years, the economic feasibility of reusing EV batteries is still uncertain today.

In recent years, the improvements in Li-ion chemistries, together with mass production have led to a cost reduction in new batteries that threatens the SL market. Up to 30 % of the price of reused batteries is determined by their repurposing process [8]. In this stage, characterization is key from a dual perspective: to ensure that reused modules are suitable for the specific application and to minimize dispersion within reconfigured batteries. The latter can be up to four times the value in new modules [3], and it may compromise the requirements of power converters [9] or even battery lifetime [10,11]. Moreover, knowledge of the degradation level of reused batteries is also necessary throughout their SL lifetime, in order to guarantee safe operation. Traditionally, Li-ion batteries are characterized by capacity and/or internal resistance in

Nomenclature		*LR*	linear regression	
		MaxE	maximum absolute error	
CC	constant current	*PC*	partial charge	
C_N	nominal capacity	*PCM*	partial charging method	
C_{RPT}	capacity	*RMSE*	root mean squared error	
CV	constant voltage	*RPT*	reference performance test	
DCIR	direct current internal resistance	*SL*	second life	
EIS	electrochemical impedance spectroscopy	*SOC*	state of charge	
EV	electric vehicle	*SOH*	state of health	
HI	health indicator	*SVR − L*	support vector regression with linear kernel	
IC	incremental capacity	*SVR − RBF*	support vector regression with radial basis function kernel	
ICA	incremental capacity analysis			

order to assess their state of health (SOH). SOH is an index of the ageing condition of batteries, and its monitoring requires several hours of testing and specific equipment and eventually the interruption of normal operation.

In the quest to optimise degradation assessment of Li-ion batteries, the estimation of their SOH has emerged as an alternative in recent years. In an initial stage, all SOH estimation methods aim to identify a characteristic parameter related to SOH, i.e., a health indicator (HI), from which SOH can be assessed. In general, two options have been addressed: experimental and model-based methods [12,13]. The first approach relies on laboratory testing to analyse ageing behaviour, covering direct measurements of HIs such as impedance measurements [14] or Ah counting [15,16], as well as indirect assessment which requires data analysis and processing to evaluate HIs, e. g. from incremental capacity analysis (ICA) [17,18], voltage response [19–21] or charging curve method [4]. Another novel approach is the assessment of stoichiometry parameters, which focuses the analysis at electrode level, thereby obtaining valuable information about degradation mechanisms [22]. Despite their accuracy, experimental methods are difficult to implement online, given that they require specific equipment and are performed in a laboratory environment, which may differ from real conditions [15,23,24]. For their part, model-based methods aim to estimate or identify HIs and can be divided into adaptive filtering algorithms, such as Kalman Filters [25], and data-driven methods, which are based on machine learning algorithms, such as Support Vector Machine or neural networks [15,26,27]. The accuracy and robustness of results, together with the shorter time series of data required make these methods more attractive for real applications. Nevertheless, complex models or HI extraction procedures lead to higher computational requirements, which may compromise the implementation of a specific SOH estimation method in battery management systems.

All SOH estimation methods for Li-ion batteries require, in an initial stage, the extraction of HIs. Li-ion battery ageing is caused by multiple mechanisms such as chemical decomposition and structural changes, as well as by their interaction, and the assessment of such features is thus not evident. Moreover, the correlation between HI and SOH influences the specific algorithms used in estimation. The trade-off between algorithms, considering accuracy and implementation easiness, and HI extraction in real applications is extremely significant in SOH estimation [28]. However, although SOH estimation has become relevant in recent years, only a few studies focus on SL batteries. The inhomogeneous characteristics of these reused batteries due to previous usage in EVs, together with the acceleration of their ageing rates related to changes in the dominant ageing mechanisms in the so-called ageing knee, motivate the specific analysis of SL batteries.

Table 1 summarizes the main contributions identified which target this issue, detailing for each case the specific HI and algorithm used, together with the application addressed, capacity fade interval and the resulting prediction error. The assessment of SOH at the repurposing stage has been addressed through direct measurements of HIs such as

Table 1
Research contributions targeting SOH estimation for SL Li-ion batteries.

Reference	Health indicator	Algorithm	Application	Capacity fade interval (%)	Maximum prediction error (%)
[14]	EIS	Linear regression	Repurposing	5–20	2
[29]	PCM	Support vector machine and K-means algorithm	Repurposing	17–40	3
[30]	ICA	Linear regression, ordinary least square, ridge regression	Repurposing	15–35	3
[15]	PCM	Weighted least squares support vector machine	Online	20–55	1.85 (RMSE)
[4]	EIS, charging curve, ICA and AFD	Linear regression	Online Offline	6–38	1.5

electrochemical impedance spectroscopy (EIS) [14], with a SOH prediction error below 2 %, or Ah counting in partial charging method (PCM) [29], which allowed a capacity estimation accuracy of within 3 %. For its part, [30] used indirect HIs from ICA to achieve 3 % prediction accuracy in SOH estimation. When it comes to online SOH assessment, [15] estimated SOH with a maximum error of 1.85 % under extended SL ageing using Ah counting in PCM, while [4] assessed average Fréchet distance (AFD) in the constant current section of the charging curve, obtaining 1.5 % of SOH estimation error. This latter work addressed both online and offline SOH estimation. It should be noted that the cells' capacity, format, and chemistry analysed in the contributions might vary.

As can be seen from Table 1, only a few steps have been taken with regard to SOH estimation in SL Li-ion batteries. Most studies focus on the repurposing stage, and there is clearly a lack of a complete SL lifetime assessment. Overall, this research work is supported on two grounds: the importance of simplifying SOH estimation algorithms in order to facilitate their implementation in real applications and the literature gap

found in the analysis of HIs in SL batteries. Therefore, this contribution aims to assess the selection of HIs for SOH estimation in reused Li-ion batteries from EVs. Experimental data will be extracted from modules retired from real EVs, adding valuable information for the economic and technical viability of the SL market. The paper is organized as follows. Section 2 details the experimental procedure, describing the Li-ion modules used and the experimental setup. An overview of HI extraction is provided in Section 3, together with the SOH estimation procedure. Section 4 presents and discusses the results covering the repurposing stage and the complete SL lifetime. Moreover, a comparison of different estimation algorithms with a given HI is carried out in this section. Finally, Section 5 draws the main conclusions of the work.

2. Experimental procedure

2.1. Module description

The six Li-ion modules under study in this work were specially designed for automotive purposes, in particular for the Nissan Leaf EV. Each module is composed of four pouch-type cells of nickel and manganese oxide cathode (LMO/LNO) and graphite anode. The cells are assembled in two parallel-connected pairs associated in series (2s2p). Three external terminals are available in the modules: positive, middle point and negative, in such a way that 2p cells are the smallest testing unit. The nominal capacity (C_N) of the modules is 66 Ah, and their maximum, minimum, and nominal voltages are 8.3 V, 5 V, and 7.5 V, respectively. The EV history of the modules is unknown, as this is not provided by the manufacturer. Fig. 1 shows some of the modules under test in the laboratory setup. The cells have only been used in the EVs, being therefore at the beginning of their SL.

2.2. Experimental setup

The tests are carried out at 2p cell level between the positive and middle point terminals. For ease of reading, the 2p cell connection will hereinafter be referred to as cell. The experimental procedure of this contribution consists of two main sets: reference performance tests and cycling ageing tests.

2.2.1. Reference performance test

The reference performance test (RPT) is composed of capacity and direct current internal resistance (DCIR) measurements. The capacity test consists of two full charge-discharge cycles at C/3 between the voltage limits of the cell. C is defined according to the nominal capacity. The charging procedure is a constant current (CC) pulse until the maximum cell voltage followed by a constant voltage (CV) phase with a

Fig. 1. Example of Nissan Leaf modules under test and experimental test bench.

cut-off current of C/20, while the discharge procedure is CC. The actual capacity of the cell (C_{RPT}) is determined from the capacity discharged in the second cycle. The RPTs are carried out at a controlled ambient temperature of 25 °C $\pm$ 1 °C. *Prior* to the initial test, a rest time of 4 h is set at the given temperature, and the cell is discharged at C/3 with a CC pulse down to their minimum voltage. For their part, the DCIR tests starts with a CC full charge at C/2. Then, the cell is discharged at C/2 with a CC pulse until it reaches 90 % of its state of charge (SOC). After a 1 h rest, the procedure is repeated until the next SOC level is reached. The DC internal resistance is calculated from the voltage and current after 10 s of discharge pulse and their values at the end of the rest period. The process is performed at SOC levels of 90 %, 70 %, 50 %, 30 % and 10 %.

2.2.2. Ageing test

The ageing test consists of a continuous cycling with CCCV charge and CC discharge at 1C between cell voltage limits, with a cut-off current of C/20. The test is performed at a controlled ambient temperature of 25 °C $\pm$ 1 °C. An RPT was performed every 250 cycles.

Fig. 2 shows a sequence example of RPT, with the corresponding capacity and DCIR measurements, and cycling ageing test performed in one of the cells under test.

The test bench used, shown in Fig. 1, consists of a battery tester and a climatic chamber. The battery tester is rated at 5 V and 50 A on each channel, with an accuracy within ± 0.1 % of the full scale. The climatic chamber allows a temperature range from -30 °C to $+180$ °C, with measurement precision of ± 0.5 °C. Data processing and computations are performed with the Matlab R2020a software.

3. Health indicator extraction and SOH estimation

The estimation of SOH consists of two main steps. First, it is necessary to extract HIs that provide useful information regarding ageing. Given the complexity of degradation mechanisms in SL Li-ion batteries, and the eventual appearance of the ageing knee, the selection of such indicators is no trivial matter. Once the specific HI is identified, a correlation with SOH is analysed in a second stage. Thus, this section covers both steps, describing the HI extraction and the SOH estimation procedures.

3.1. Health indicators

The extraction of HI for SOH estimation is regarded as one of the main challenges in this field nowadays [26]. Robustness to ageing and operating conditions, together with accuracy and easiness of extraction, are characteristics sought in HIs. This, together with the reused character of the cells under study, motivates the analysis of different extraction methods. From each method, the number of HIs obtained depends on the information available and their tailoring to the specific characteristics of the cells. Hence, four HI extraction methods are selected in this contribution: incremental capacity, partial charging, internal resistance and amount of charge in the CC and CV stages. Among other alternatives, the encouraging results of these methods in previous literature motivated their choice for SL batteries. All the HIs are extracted under similar measurement conditions, according to the RPT procedure described in subsection 2.2.1. Therefore, the dependence on current or temperature in the HI extraction does not come within the scope of this work.

3.1.1. Incremental capacity

ICA has been reported as a promising technique to estimate SOH in SL Li-ion batteries [31], with accurate results at acceptable computational costs. Based on the differentiation of capacity against voltage on a CC charge, ICA makes it possible to track the characteristic peaks and valleys, which can be used as HIs to estimate SOH. In real operation, while the discharge current is normally defined by the load, the charging
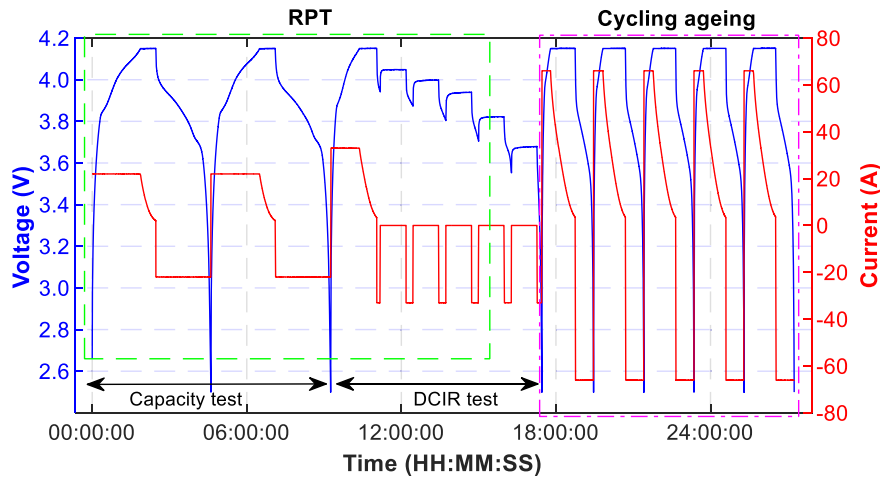
Fig. 2. Cell voltage and current signals during the RPT and cycling ageing (voltage plotted on the left axis and current on the right axis).

current is usually constant. Therefore, this method is of great interest when it comes to SOH estimation. Moreover, when performed at low currents, ICA makes it possible to identify underlying degradation mechanisms in Li-ion cells, which, although not coming within the scope of this contribution, could also be seen as a further advantage of this technique to be used in SOH assessment. Nevertheless, the initial SOC of the cell may compromise the identification of some indicators [32], and the method requires data processing to filter the curve in order to get HIs.

In this contribution, the incremental capacity (IC) curve is extracted from the second charge of the capacity test in the RPT on its CC stage. The sampling time interval is 1 s. Each charge is split into 300 sections of equal time, considering this number as a compromise between the measurement noise and IC detection. For each section, named n to n + 1, voltage and capacity change are obtained, computing the IC as the differentiation of the battery charging capacity (Q) against the voltage (V), according to Eq. (1).

$$IC = \left(\frac{dQ}{dV}\right)_n = \frac{Q_{n+1} - Q_n}{V_{n+1} - V_n} \tag{1}$$

Measurement noise in the IC curve is mitigated through a moving average filtering of 12 points. This solution is found to be the best compromise between accuracy and simplicity. The peak and valley identification is performed on the filtered IC curves using the 'findpeaks' function in Matlab. The minimum distance between peaks and valleys is

set to 30 points, and the minimum height to 5 points.

Fig. 3 shows the IC curves of the six cells (C 1 to C 6) under study in this contribution at the beginning of the test, i.e., at their repurposing stage. As can be seen, two peaks (P 1 and P 2) and a valley (V 1) are identified according to the procedure described in this subsection. This is consistent with a previous work performed with similar SL modules [31]. From each of these characteristics, the IC magnitude and the corresponding voltage will be kept as HIs. Hence, six indicators are available (HI 1 to HI 6), as is summarized in Table 2. For example, HI 1 corresponds to the IC magnitude of Peak 1 and HI 4 represents the voltage of Peak 1.

3.1.2. Partial charging method

PCM relies on the concept that the overall capacity of the cell can be estimated from a given charge measured in a specific voltage range. As in the case of ICA, this technique can be applied in normal battery

Table 2
HIs extracted from ICA.

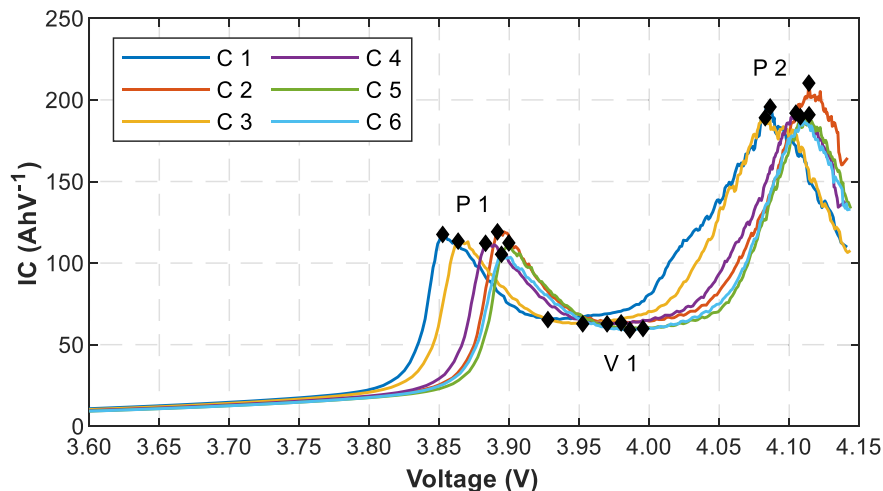| Characteristic	ICA HI	
	IC	Voltage
Peak 1	HI 1	HI 4
Peak 2	HI 2	HI 5
Valley 1	HI 3	HI 6

Fig. 3. IC curves of the six cells at the beginning of their SL.

operation, given that current is usually constant during battery charging. One of the main advantages of PCM is its simplicity, as it is based on Ah counting and does not require data processing.

In this work, partial charging data are obtained from the second cycle of the capacity test in the RPT in its CC stage. The voltage range analysed is from 3.7 V to 4.15 V, given that the most significant changes in IC occur within these values, as shown in Fig. 3. The entire voltage range is divided into fractions of 50 mV and, as a result, 45 voltage windows are identified. At each interval, the corresponding charge in Ah is extracted as the indicator for SOH estimation (HI 7 to HI 51). Table 3 summarizes the HIs extracted through PCM, detailing for each interval, the corresponding low (V_{LOW}) and high voltage (V_{HIGH}). For instance, HI 7 corresponds to the partial charge extracted from 3.70 V to 3.75 V.

Fig. 4 shows an example of HI extraction for a given SL cell at the beginning of its life (Fresh) and after being aged (Aged) through PCM. For exemplification, the voltage range between 3.9 V and 4.1 V, corresponding to HI 40 is plotted.

3.1.3. Internal resistance

Capacity and internal resistance are correlated in a Li-ion cell, in such a way that degradation leads to capacity fade and resistance increases. Given the simplicity of measurement and its possibilities in real applications, DCIR is considered as HI to estimate SOH. The value of DCIR depends on the SOC of the cell, in such a way that extremely high or low levels increase the internal resistance [33]. Therefore, DCIR is considered as HI at various SOC. More precisely, in this work, the DCIR test in RPTs is the extraction method for these HIs, according to the procedure described in Section 2.2.1. Hence, five HIs are available, from the corresponding SOC levels of the test (90, 70, 50, 30, and 10 %), which are named HI 52 to HI 56.

Table 4 describes the specific SOC of each HI, in such a way that HI 52 is the DCIR measured at the discharge pulse of 90 %.

3.1.4. Charge in CC and CV stages

The study of the CC and CV stages from a specific charge makes it possible to extract different HI, such as energy, temperature or the slope of the curve [28]. In this contribution, the corresponding charge of each stage will be considered, given the extraction simplicity. As for ICA and PCM, this method can be applied in normal battery operation given that the charging current is usually controlled. In this contribution, the second charge of the capacity test in the RPTs is considered. For a given charge, the corresponding CC and CV charges are extracted as shown in Fig. 4. Thereby, the HI related to the charge in the CC stage (Q_{CC}) is named HI 57, while HI 58 corresponds to the charge in the CV stage (Q_{CV}).

3.2. SOH estimation

The aim of this work is to assess different HI for reused cells during their SL lifetime. SOH is a reference of the degradation state of Li-ion batteries, and it can be related to their capacity, energy or power capabilities. In this work, SOH will be defined as the ratio between the actual capacity, measured during the capacity test of a given RPT and the nominal value, according to Eq. (2), and expressed as a percentage.

$$SOH\ (\%) = \frac{C_{RPT}}{C_N} \cdot 100 \tag{2}$$

Two of the main metrics to evaluate the goodness of a HI are its dependency on SOH and its robustness to ageing. In order to assess the first condition, each of the 58 HIs previously described will be analysed separately. Aiming to facilitate the procedure, HIs that show a linear correlation with SOH will be targeted. Therefore, their correlation with SOH will be evaluated through linear regression. The goodness of fit will be assessed considering the estimated and measured value of SOH by means of root mean square error (RMSE) and maximum absolute error (MaxE). Therefore, the best indicators for SOH estimation among the proposed alternatives will be selected.

HI selection is the first stage in the development of all SOH estimation methods and plays a key role in determining the specific algorithm. Once the most suitable indicators are detected, SOH estimation will be assessed by means of different methods. Li-ion batteries are complex systems, and the estimation of their SOH is usually a non-linear problem. Nevertheless, if the HIs are linearly related to SOH, a simple linear regression is sufficient. Therefore, two different algorithms will be considered: linear regression (LR) and support vector regression (SVR). LR is one of the most targeted SOH estimation algorithms given its simplicity. The objective function of this algorithm is $SOH\ (HI) = a \cdot HI + b$, being the coefficients a and b adjusted by the least squares method. However, the accuracy of this algorithm is compromised when it comes to non-linear problems, and it may lead to overfitting problems [26]. For its part, SVR is a generalization algorithm that recognizes patterns. Despite its computational complexity, SVR has become a widely-used approach for SOH estimation, as it can be used for non-linear problems and requires fewer data points for training than other ML algorithms [26]. The objective function of LR is targeted in this case by solving a convex quadratic problem, which is normally simplified by introducing the kernel function [13,15]. In this contribution, linear (SVR-L) and radial (SVR-RBF) kernel functions will be used in SVR, given that they are commonly used to deal with non-linear problems.

The SOH estimation procedure will be carried out in two steps. First, the SOH models will be trained by means of cross validation, in order to increase their robustness. For a given model, if only the RMSE of the training set was considered, the accuracy would be overestimated, as the RMSE when predicting a new dataset would be greater. Therefore, a separate validation set is drawn from the same population as the training samples, without being used for parameter estimation. The complete cross validation process is:

   i. Random division of the data into k parts, named folds, of equal size.
   ii. Training the model with k-1 folds. Parameters are thereby estimated.
  iii. Testing the model in the remaining fold, computing the corresponding RMSE and MaxE.

Table 3
HIs extracted from PCM and their lower and upper voltage.

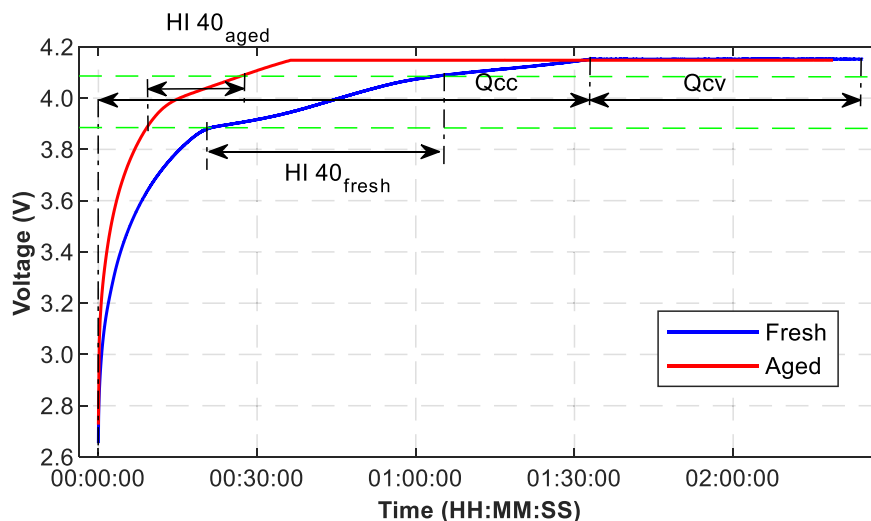| V_{HIGH} (V)	V_{LOW} (V)								
	3.70	3.75	3.80	3.85	3.90	3.95	4.00	4.05	4.1
3.75	HI 7								
3.80	HI 8	HI 16							
3.85	HI 9	HI 17	HI 24						
3.90	HI 10	HI 18	HI 25	HI 31					
3.95	HI 11	HI 19	HI 26	HI 32	HI 37				
4.00	HI 12	HI 20	HI 27	HI 33	HI 38	HI 42			
4.05	HI 13	HI 21	HI 28	HI 34	HI 39	HI 43	HI 46		
4.10	HI 14	HI 22	HI 29	HI 35	HI 40	HI 44	HI 47	HI 49	
4.15	HI 15	HI 23	HI 30	HI 36	HI 41	HI 45	HI 48	HI 50	HI 51

Fig. 4. Example of partial charge extraction (HI 40) in a SL cell at the beginning of the test (Fresh) and after being aged (Aged) and CCCV charge stage description.

Table 4
HIs extracted from DCIR measurements and their corresponding SOC.

SOC (%)	90	70	50	30	10
HI	HI 52	HI 53	HI 54	HI 55	HI 56

iv. Repeating the process k times, in such a way that all the folds are used as train and test sets.

v. The cross-validation error is then found as the average of the k testing errors. In addition, the final parameter values are computed as the average of the k training models.

Secondly, the models will be validated in extra data sets from other cells, obtaining the corresponding validation RMSE and MaxE.

4. Results and discussion

The assessment of HI for SOH estimation is held in two stages: at the repurposing stage and during SL operation. In both cases, six Nissan Leaf cells removed from real EVs are compared. The HIs were obtained according to the procedures described in Section 3.1. Considering the specific information available from each method and their adjustment to the cells under study, a total of 58 HIs are selected. It is important to note that the HIs are compared under similar measurement conditions, and therefore the dependence on current and temperature is not considered. Once the HIs are evaluated, the most robust HI with ageing will be selected and used for SOH estimation with different algorithms.

4.1. Repurposing stage

In compliance with automotive standards, Li-ion battery packs are normally retired from EVs when their SOH reaches 80 to 70 %. However, their constituent cells usually perform under different operating conditions when operating in EVs. This may lead to a dispersion on their internal parameters, as detected in previous studies with similar cells [3,34]. Hence, the six retired cells, named C 1 to C 6, are first tested under the RPT described in Section 2 in order to assess their condition at the beginning of their SL. Table 5 shows the results of the corresponding RPT. Capacity is expressed both in Ah and in terms of SOH. For its part, the DCIR at 50 % of SOC is obtained as a representative measurement.

As can be seen in the table, the SOH measured ranges from 62.8 % to 71.2 %. The average value of SOH is 66.8 %, slightly below the automotive retirement limit. The correlation between DCIR and SOH can

Table 5
Capacity, SOH and DCIR at 50 % of SOC of the six Nissan Leaf cells at their repurposing stage.

Cell	C 1	C 2	C 3	C 4	C 5	C 6
Capacity (Ah)	47.01	45.22	44.65	44.23	41.99	41.44
SOH (%)	71.23	68.51	67.65	67.01	63.62	62.79
DCIR @ 50 % SOC (mΩ)	1.83	1.99	2.05	2.03	2.15	2.47

also be observed as, in general, the higher the capacity, the lower the internal resistance. The nominal value of DCIR is unknown, as this is not provided by the manufacturer, and therefore the relative increase cannot be determined.

From the RPT performed at the repurposing stage and through the procedures previously described, the 58 HIs are extracted (HI 1 – HI 58), and the SOH of the cells is estimated for each case by LR. This estimation is related to the SOH measured in the RPT, computing thereby the RMSE. Fig. 5 shows the results obtained for the 58 HIs in terms of RMSE (Fig. 5a) and MaxE (Fig. 5b). As can be seen, the RMSE ranges from 0.2 % of HI 3 (ICA: IC in Valley 1) to 3.8 % of HI 51 (PCM: 4.1 V – 4.15 V), with an average value of 1.6 %. For its part, the average MaxE is 2.5 %, ranging from 0.6 % to 5.1 %. Given the importance of reducing the internal dispersion of reconfigured batteries to ensure safety and to extend the SL lifetime, specific accuracy could be desirable. Hence, it is found that 15.5 % of the 58 features analysed lead to less than 1 % of RMSE. The main part of the features, 69 %, make it possible to estimate SOH with between 1 and 2 % of RMSE.

When it comes to the repurposing stage, the reduction of measurement times is key to lowering costs. Therefore, the required testing time to obtain the HIs is also shown in Fig. 5c. In this plot, HIs are grouped based on the extraction method. For example, to obtain indicators through ICA, the required testing time ranges from 25 to 81 min. Post-processing data timing is not considered. As can be seen, DCIR is the fastest HI to be measured, with a test time of less than 1 min, while the longest time, around 99 min, is required in the CC and CV charge. When relating time and RMSE, in general for HIs involving Ah counting, the greater the time, the lower the RMSE, as could be expected. For example, if a measurement time of over 25 min is set, the RMSE is lower than 1.85 % in PCM. This is also the case of CCCV charge at the reconfiguration stage, where Q_{CV} measurement requires less than 30 min with around 3.0 % of RMSE and Q_{CC} almost 100 min to obtain half the RMSE. Nevertheless, this is not the case of ICA, where no correlation between measurement time and RMSE is found.

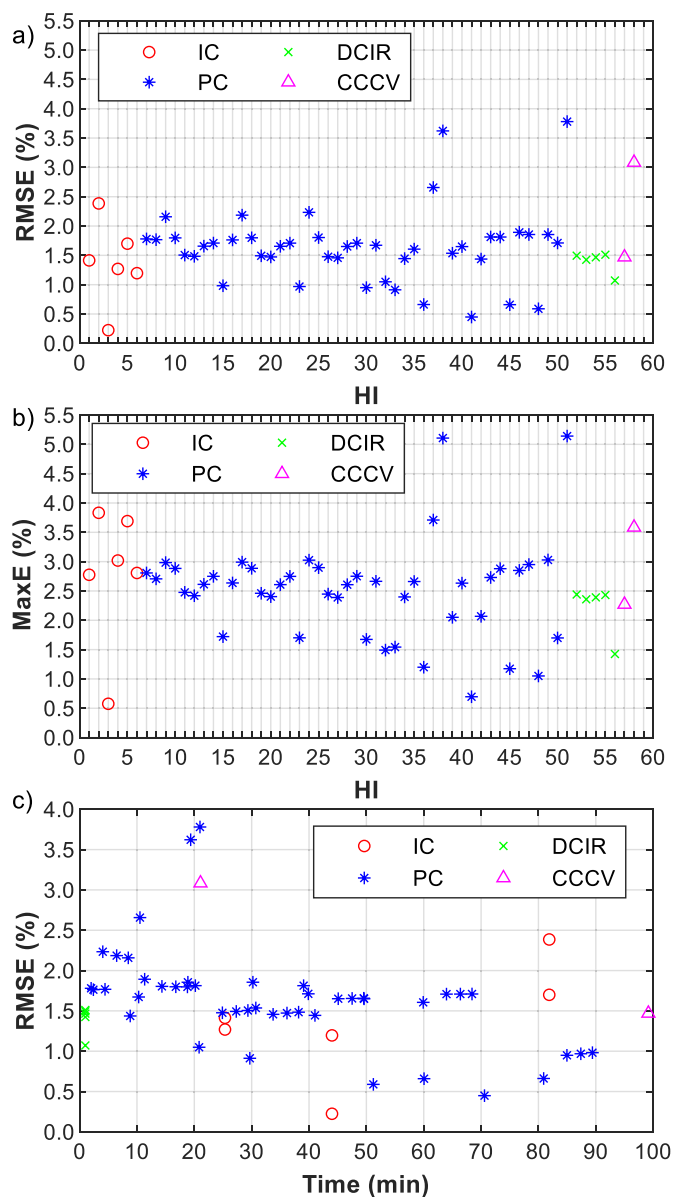Looking at each extraction method separately, ICA is found to have

Fig. 5. a) RMSE, b) MaxE and c) Time of measurement of HIs at the repurposing stage.

the best results over the 58 candidates, with an RMSE of 0.2 % achieved with IC in Valley 1 (HI 3). In previous work related to this technique, this valley was also found to be a good HI for SL cells [31]. All the HIs extracted with this technique showed an RMSE of less than 2.5 %. Regarding the few research contributions identified that cover SOH estimation of reused batteries, summarized in Table 1, the heterogeneity of capacity, format and chemistry of the cells analysed allows only a general comparison of the proposed HIs. Bearing this in mind, four of the six HIs obtained from ICA showed similar or better accuracy results than previous contributions that targeted this extraction method at the reconfiguration stage [30].

Regarding PCM, the accuracy of the HIs depends on the specific voltage range. Fig. 6 details the results of RMSE obtained for each charge at the corresponding V_{LOW} and V_{HIGH}. As can be seen, the best accuracy is obtained when the highest voltage available is reached, with RMSE lower than 0.95 %. Good results are also obtained in HI 33 (3.85 V – 4 V), with 0.90 % of RMSE and in HI 32 (3.85 V – 3.95 V), with 1.05 %. Regarding MaxE, six of the HIs allow to estimate with less than 1.5 %, and the main part of the indicators are below the 3 % of maximum

prediction error stated in other research studies that use this method for a similar purpose [29]. As can be seen in Fig. 6, there are significant accuracy differences in adjacent voltage ranges, specially between 3.85 V and 3.9 V for an upper voltage of 4.0 V. A possible reason for this is the influence of charge distribution depending on voltage in the cells under study, which can be assessed by IC curves. As Fig. 3 shows, there is a slight mismatch between the IC curves of the six cells at the beginning of their SL. Hence, the best results of HIs from PCM are obtained in voltage ranges that cover similar IC areas, such as the whole Peak 1 of all the HI 32 and HI 33. On the other hand, the worst results are obtained in HI 38 and HI 51, both HIs corresponding to voltage ranges with a mismatch in IC curves of the cells. Therefore, it can be concluded that PCM features show better results when applied in voltage ranges with similar IC curve behaviour. It is also noteworthy that with V_{LOW} from 3.7 V to 3.8 V, the RMSE pattern is similar for all the upper voltages considered. This corresponds to voltages below the first peak identified by ICA (Peak 1).

Considering DCIR measurement as extraction method, SOH is estimated with less than 1.5 % of RMSE requiring around 1 min of measurement. This low testing duration is an advantage in terms of optimizing repurposing times. Nevertheless, given its small magnitude, DCIR requires precise equipment to be determined and it can be highly influenced by measurement variability. The maximum errors obtained with this method are lower than 2.4 %. The most similar contribution gathered in Table 1 focused on impedance measurement through EIS, with the subsequent instrument requirement, and achieved error values lower than 2 % [14]. Finally, charge in CC stage shows good RMSE results, around 1.5 % of RMSE, but requires long testing times. For its part, charge in CV stage can be measured faster than in CC stage at the repurposing stage but may not always be possible in real operation. Furthermore, many battery management systems perform balancing actions during this CV stage, which might also affect HI extraction.

From this analysis, a first insight on HIs for SOH estimation on SL batteries is carried out. Nonetheless, given the complexity of assessing degradation in Li-ion batteries, which eventually suffer from an acceleration in the ageing trends, an extended analysis on the HI covering a wider SL lifetime range is of great interest. Therefore, the next section evaluates the HIs and SOH estimation during extended SL operation.

4.2. Extended second-life operation

Robustness to ageing is key in HI, especially in SL batteries. In order to evaluate this attribute, the six Nissan Leaf cells were aged according to the test described in Section 2.2.2. Fig. 7 shows the SOH measurements from RPTs with the corresponding Equivalent Full Cycles (EFC) during the test. EFC is defined as the sum of the entire Ah throughput during the ageing test related to the nominal capacity of the cells. Further information about the test results can be found in [5]. The SOH range covered during the ageing test goes from 71.2 % to 24.4 %. As shown in the figure, in the initial ageing stages, the cells show quasi-linear capacity fade with slightly different slopes. During the second stage, there is a change in the ageing trend, in the so-called ageing knee, where the degradation accelerates. From this point, there is a change in the main ageing mechanisms of the cell, which involves higher safety risks in operation. Therefore, SL lifetime should be limited before the apparition of such ageing knee. This second stage starts between 45 % and 49 % of SOH, depending on the tested cell.

The 58 HIs were tracked during the ageing test in the corresponding RPTs. However, HIs extracted from ICA could not be identified in advanced stages of degradation. When it comes to HI identification, IC curves vary with ageing, with Peak 2 vanishing below 56 % of SOH. For SOH values lower than 47 %, it was not possible to identify any peak or valley with the C-rate used during the RPT capacity measurement. In previous research with similar cells, it was found that increasing testing currents lead to feature vanishing, especially at low SOH, so lower C-rates would be advised in these cases [31]. This loss of HIs could be alternatively used as an approach for SOH estimation. For example, in
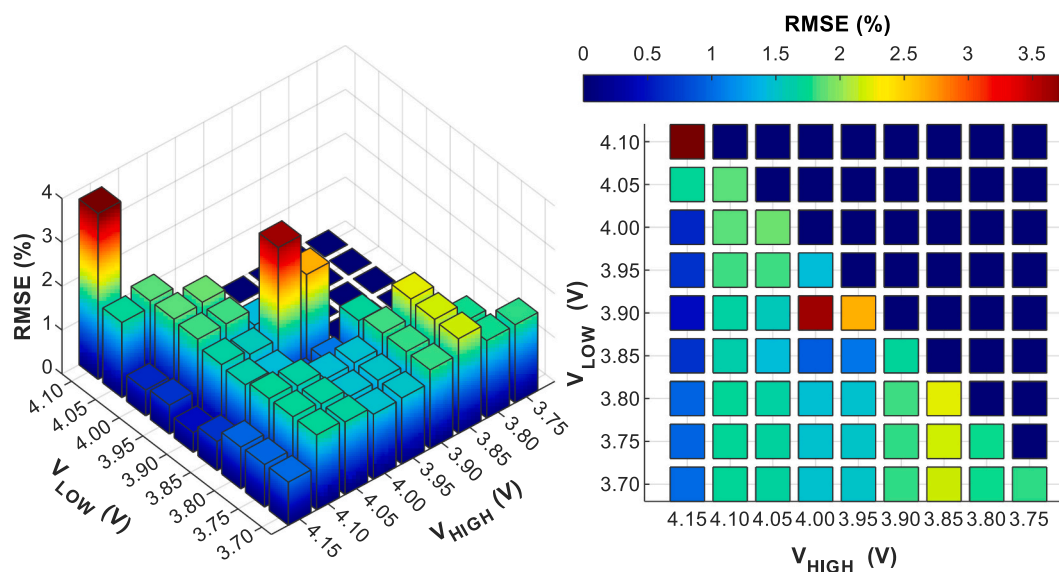
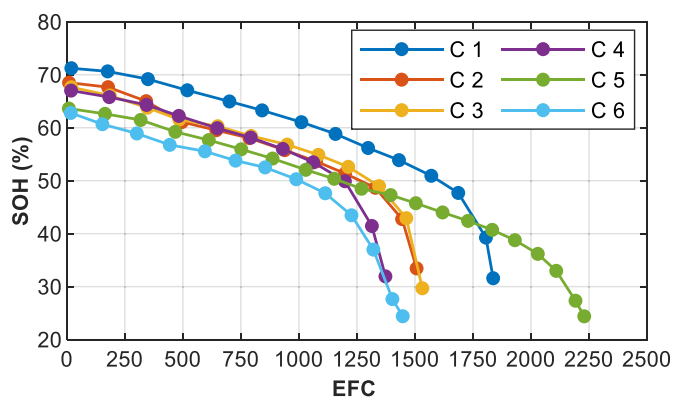**Fig. 6.** RMSE of HIs obtained from PCM at repurposing stage.

Fig. 7. SOH measured during the cycling ageing test in the six Nissan Leaf cells.

the cells under study, ICA features could not be tracked below the ageing knee, thereby making it possible to detect it. Given the complexity of ageing assessment in SL Li-ion batteries, a deeper insight on HI depending on the SOH level is carried out. Hence, three SOH ranges were defined: SOH range A, with values greater than 60 %, range B, covering middle SOH values between 50 and 60 %, and range C, which considers SOH values below 50 %. The number of RPTs performed in SOH ranges A, B and C were 25, 29, and 28 respectively.

The HIs were assessed with the same procedure as in the repurposing stage. The SOH was thus estimated through LR from the corresponding HI, and the error considering the actual value was computed. Fig. 8 presents the RMSE of each HI using data from each of the three SOH ranges separately and all together. As can be seen, the worst results are obtained when all the SOH range is covered, with an average RMSE value of 4.7 % in the 58 HIs. However, when a specific range is analysed, SOH estimation improves. Therefore, in range A, the RMSE varies from 0.7 % to 3.2 %, with an average value of 2.2 %. When SOH decreases, the estimation improved, with RMSE in range B between 1.2 % and 2.7 %, and an average value of 1.6 %. Capacity fade rate was found to be more homogeneous in this range between the cells under test, which could explain the better results obtained. Finally, the worst estimation was obtained in SOH range C, with an average value of 3.5 % and values from 0.9 % to 8.0 %. This could be related to the inhomogeneous acceleration in the degradation rate of the cells, as for example the ageing knee was detected at SOH of 49.4 % in cell C 3, while in cell C 5 this

point appeared at 32 % of SOH.

When assessing extraction methods of HIs throughout ageing, ICA is found to be the best in the lowest SOH range, but it should be noted that the corresponding HIs vanished below a specific SOH value, and less data were thus considered compared to other methods. For its part, PCM shows the best results in SOH range B. As was observed at the repurposing stage, the best results in PCM were obtained in voltage ranges with similar IC curve behaviour. Given that Peak 2 fades and vanishes in this SOH range, the resulting increase in homogeneity of IC curves could be related to the better SOH estimation results. Regarding DCIR, this method performs best in SOH range A. This could be explained with the correlation between DCIR and capacity during SL lifetime. During SL ageing, DCIR increases linearly with Ah throughput in early stages, with a similar trend than capacity fade. However, the degradation rate of DCIR accelerates in a second phase, while capacity loss remains linear. Finally, capacity fade changes its trend after the ageing knee [5]. Therefore, DCIR is advised as HI in early stages of SL.

To summarize, Table 6 gathers the best HIs for each range, specifying in each case the RMSE and MaxE obtained. As can be seen, in general, PCM is the best extraction method for HIs in SL Li-ion cells, with errors below 1.4 % in SOH range A, 2.2 % in B and 3.4 % in C. In this latter SOH range, although ICA indicators (HI 1, HI 2, HI 5 and HI 6) showed good RMSE results, it should be noted that less data were available due to feature vanishing. HI 3 and HI 4 could not be tracked for SOH range B and C. From this analysis, it can be stated that it is worthy to focus on different HIs depending on the specific SOH range. On the other hand, regarding ageing robustness, PCM also made it possible to track the best indicators. More precisely, considering all RPTs available, HI 40 allowed SOH estimation within 71.2 % to 24.4 % of SOH with 1.9 % of RMSE, and both HI 34 and HI 13 with 2.1 %. Despite the literature gap on SL SOH estimation, as already mentioned, some discussion can be held from the contributions identified in Table 1. PCM was used in [15] within a SOH range from 80 % to 45 %, achieving 1.85 % of RMSE, but targeting online estimation, while [4] achieved 1.5 % of maximum error covering SOH from 92 % to 61 % with AFD method.

4.3. SOH estimation: Case study

The selection of HIs influences the requirements for SOH estimation algorithms. In this context, this subsection aims to evaluate different mathematical approaches. From the previous analysis, the best HIs depending on the SOH range, as well as the most robust HIs to ageing
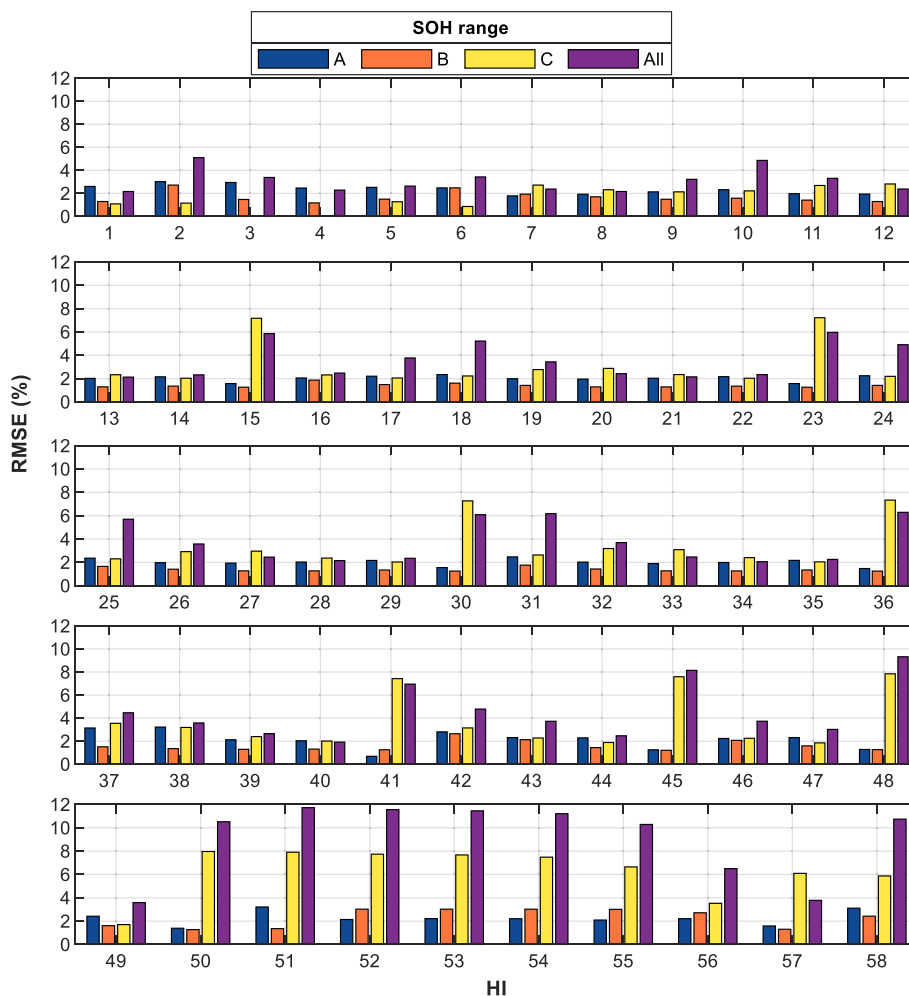
Fig. 8. RMSE of the 58 HIs depending on SOH range.

Table 6
Best HI depending on SOH range with the corresponding measurement method, RMSE and MaxE.

SOH Range	Measurement method	HI	RMSE (%)	MaxE (%)
	PCM	HI 41 (3.9–4.15 V)	0.69	1.36
A	PCM	HI 45 (3.95–4.15 V)	1.25	2.71
	PCM	HI 48 (4–4.15 V)	1.28	3.02
	ICA	HI 4 (voltage Peak 1)	1.18	1.26
B	PCM	HI 45 (3.95–4.15 V)	1.21	2.20
	PCM	HI 36 (3.85–4.15 V)	1.25	2.46
	PCM	HI 40 (3.9–4.0 V)	1.92	3.37
C	PCM	HI 34 (3.85–4.05 V)	2.06	4.29
	PCM	HI 13 (3.7–4.05 V)	2.13	4.24
	PCM	HI 40 (3.9–4.0 V)	1.92	5.59
All	PCM	HI 34 (3.85–4.05 V)	2.06	4.73
	PCM	HI 13 (3.7–4.05 V)	2.13	5.02

during all SL lifetime were identified. In this case, the comparison will be carried out considering the same HI so that the accuracy of estimation algorithms with the same input is assessed. Among the options presented in Table 6, HI 34 (PCM: 3.85–4.05 V) is selected, given its robustness to different ageing stages.

Therefore, following the procedure described in Section 3.2, SOH models are first trained and tested through cross validation with the data sets from four of the cells, and subsequently validated with the two remaining cells. Three algorithms are considered: LR, SVR-L and SVR-RBF, and for each case, the k-fold division for cross validation is performed with five groups. In order to assess different evaluation cases, four scenarios are defined: with SOH validation data included in model data (Scenario 1), with values outside of the lower (Scenario 2) or higher (Scenario 3) bound and lying out of both limits (Scenario 4). Thereby, all cells are to be considered for validation. Table 7 describes each scenario, detailing the specific validation cells and the SOH range of model and validation data sets.

Fig. 9a shows the correlation between the HI and SOH in Scenario 2, with the training data set and the results of the SOH estimation depending on the algorithm in the validation cells. As can be seen, the HI depends linearly on the SOH in almost all the SOH range. It is only below

Table 7
Validation scenarios for SOH estimation with the corresponding cells and SOH ranges.

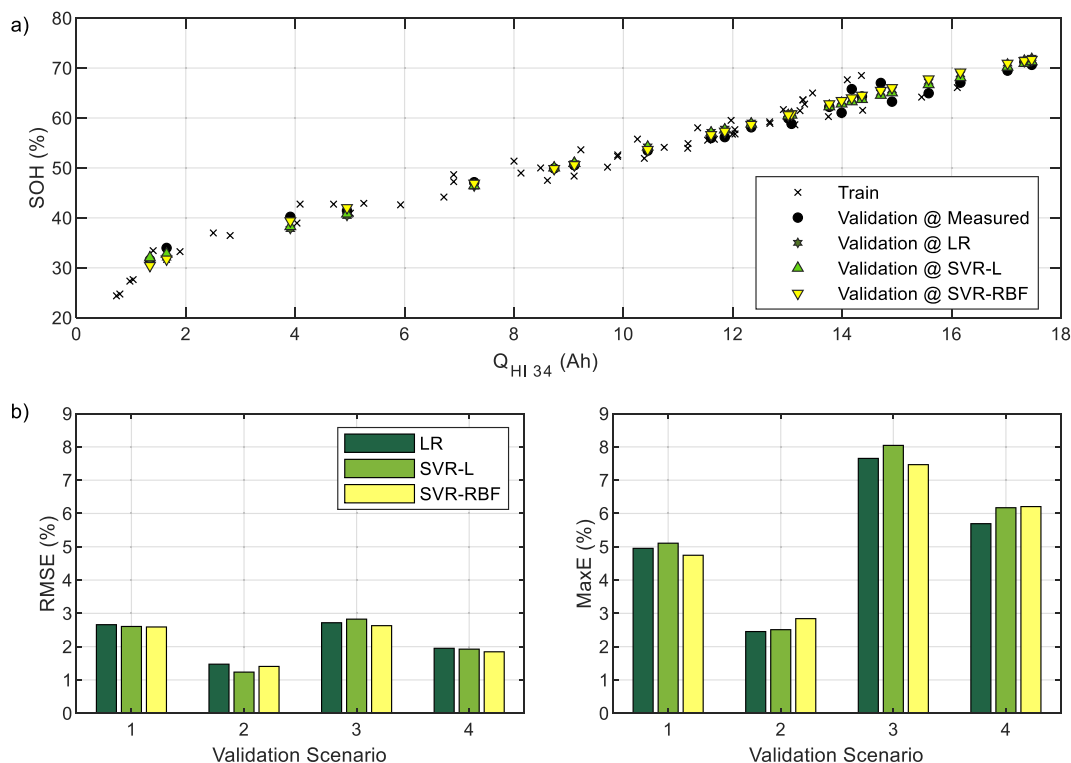| Validation scenario	Validation cells	SOH range (%)	
		Model	Validation
1	C 2, C 3	71.2–24.4	68.5–31.7
2	C 1, C 4	68.5–24.4	71.2–31.6
3	C 5, C 6	71.2–31.6	63.6–24.4
4	C 1, C 6	68.5–24.8	71.2–24.4

Fig. 9. SOH measured during the cycling ageing test in the six Nissan Leaf cells.

35 % of SOH that the overall capacity of the cell decreases faster than the charge used as HI. Given that SL operation should be restricted to degradation stages above the ageing knee for security reasons, the HI selected makes it possible to assess the SL lifetime in the case under study.

Fig. 9b shows the RMSE and MaxE obtained in the four validation scenarios with the different SOH algorithms. In terms of RMSE, accuracy values ranging from 1.24 % were obtained with SVR-L in Scenario 2, to 2.80 % in Scenario 3 with the same algorithm. Regarding MaxE in the validation set, values vary from 2.45 %, achieved with LR in Scenario 2, up to 8.05 %, resulting from SVR-L in Scenario 3. The variations observed between the validation cases may be due to two reasons. On the one hand, the existing dispersion related to SL cells should be highlighted. For example, considering Scenario 1, with SOH validation values within training data, RMSE is reduced to 1.57 % with LR if C 3 and C 4 are used. Capacity fade in C 2 has an irregular trend at the beginning of the test, as noted in Fig. 7, which could be due to its previous usage conditions. As a result, some outlier points are detected around 60 to 70 % of SOH, which worsen the estimation results in the validation stage. On the other hand, the aforementioned loss of linearity with SOH of the HI in low SOH levels leads to worse accuracy results in this area. This is compounded if the validation data are out of the lower SOH train bound, as can be noted in Scenario 3, which shows the highest validation errors. On the contrary, if cells are assessed at early stages of degradation, estimation accuracy improves even if data are out of the training set, since the HI is strongly linear with SOH. This can be observed in Scenario 2. The estimation in Scenario 4 leads to intermediate results, with 1.85 % of RMSE and 6.20 % of MaxE applying SVR-RBF algorithm. This can be also explained considering the loss of linearity at low SOH levels.

As can been noted, for a given scenario, there are only slight accuracy deviations between the three methods analysed. In general, SVR-RBF delivers the best estimation results, improving the RMSE by up to 5.40 %, in three of the four scenarios considered. Nevertheless, the complexity of the calculations required for this algorithm result in

higher computation times. Considering the average values measured for each algorithm in the four validation scenarios, SVR-RBF requires 626.80 s for model training and validation, while SVR-L and LR need 0.31 and 0.06 s, respectively. When evaluating the impact of such an increase of computational times in accuracy, it is found that the average RMSE decreases from 2.2 % using LR to 2.1 % with SVR-RBF, while MaxE increases, going from 5.2 % using LR to 5.3 % with SVR-RBF. Given the slight accuracy increase noticed with SVR-RBF and the importance of the trade-off with computational times, it can be concluded that it is not worthwhile using such complex algorithms for the case under study. From the research contributions identified in Table 1, [14,30] considered LR as well but applied only at the repurposing stage, obtaining 2 % and 3 % of MaxE respectively, while [4] used it both online and offline estimation until 40 % of capacity fade with errors below 1.5 %. However, in this work, data train and validation range from 71.2 % to 24.4 % of SOH, completely covering SL lifetime usage. In all of these contribution, a single HI is selected for all the SOH range tested. As an alternative approach and future line of this work, a combination of several HI depending on the degradation state of the cell could be considered.

5. Conclusions

This contribution evaluates the health indicator selection for SOH estimation in Li-ion cells from EVs during their second life lifetime. The need to optimise degradation assessment in order to ensure the economic viability of SL batteries and the identified research gap in this field motivates this study. A total of 58 HIs were analysed, extracted from ICA, PCM, CC and CV charge stages, and DC internal resistance measurements. The experimental procedure was carried out with six reused modules from Nissan Leaf EVs.

First, SOH was linearly estimated from HIs at the repurposing stage. The average RMSE of the 58 HIs was 1.6 %, and the best HI was achieved from ICA, with 0.2 % of RMSE. The fastest extraction method was DCIR measurement, with less than 1 min and RMSE lower than 1.5 %.

Secondly, the robustness of the HIs during SL lifetime was assessed. From experimental cycling in a SOH range from 71.2 % to 24.4 %, the most robust HIs were obtained from PCM, with an estimation RMSE lower than 2 %. Other HIs such as DCIR are only advisable at the early stages of degradation, while HIs from ICA vanished below 50 % of SOH.

Lastly, the scope of the HI choice in the SOH estimation algorithm is evaluated. From a given HI, and considering four validation scenarios, SOH models are trained and tested using linear and support vector regression. Results show that LR allows estimating SOH with similar results and significantly lower computation times than SVR.

Overall, this contribution highlights the importance of analysing health indicators for SOH estimation in SL Li-ion batteries. The choice of a good HI allows to simplify algorithms and to implement them in real systems. This contributes to the enhancement not only of the repurposing stage, but also of the on-board battery health assessment and lifetime prediction, thereby reinforcing the economic viability of SL batteries. As future lines of this work, two challenges are highlighted: the analysis of the robustness of the health indicators in other ageing modes and the extraction of features under different conditions.

CRediT authorship contribution statement

Elisa Braco: Conceptualization, Methodology, Software, Formal analysis, Investigation, Visualization, Data curation, Writing – original draft. **Idoia San Martín:** Conceptualization, Methodology, Investigation, Validation, Writing – review & editing. **Pablo Sanchis:** Resources, Supervision, Project administration, Funding acquisition. **Alfredo Ursúa:** Conceptualization, Writing – review & editing, Resources, Supervision, Project administration, Funding acquisition. **Daniel-Ioan Stroe:** Conceptualization, Writing – review & editing, Resources, Supervision.

Declaration of competing interest

The authors declare that they have no known competing financial interests or personal relationships that could have appeared to influence the work reported in this paper.

Acknowledgements

References

[1] International Energy Agency, Global EV Outlook 2021, 2020, https://doi.org/10.1787/d394399e-en.

[2] H. Engel, P. Hertzke, G. Siccardo, Second-life EV batteries: the newest value pool in energy storage, McKinsey Co., 2019. https://www.febiac.be/public/statistics.as px?FID=23.

[3] E. Braco, I. San Martin, A. Berrueta, P. Sanchis, A. Ursua, Experimental assessment of first- and second-life electric vehicle batteries: performance, capacity dispersion, and aging, IEEE Trans. Ind. Appl. 57 (2021) 4107–4117, https://doi.org/10.1109/TIA.2021.3075180.

[4] Q. Zhang, X. Li, Z. Du, Q. Liao, Aging performance characterization and state-of-health assessment of retired lithium-ion battery modules, J. Energy Storage 40 (2021), 102743, https://doi.org/10.1016/j.est.2021.102743.

[5] E. Braco, I. San Martín, A. Berrueta, P. Sanchis, A. Ursúa, Experimental assessment of cycling ageing of lithium-ion second-life batteries from electric vehicles, J. Energy Storage 32 (2020), 101695, https://doi.org/10.1016/j.est.2020.101695.

[6] C. White, B. Thompson, L.G. Swan, Repurposed electric vehicle battery performance in second-life electricity grid frequency regulation service, J. Energy Storage 28 (2020), 101278, https://doi.org/10.1016/j.est.2020.101278.

[7] H. Li, M. Alsolami, S. Yang, Y.M. Alsmadi, J. Wang, Lifetime test design for second-use electric vehicle batteries in residential applications, IEEE Trans. Sustain. Energy 8 (2017) 1736–1746, https://doi.org/10.1109/TSTE.2017.2707565.

[8] T. Alharbi, K. Bhattacharya, M. Kazerani, Planning and operation of isolated microgrids based on repurposed electric vehicle batteries, IEEE Trans. Ind. Inf. 15 (2019) 4319–4331, https://doi.org/10.1109/TII.2019.2895038.

[9] A. Berrueta, I.S. Martin, J. Pascual, P. Sanchis, A. Ursua, On the requirements of the power converter for second-life lithium-ion batteries, in: 2019 21st Eur. Conf. Power Electron. Appl. EPE 2019 ECCE Eur, 2019, pp. 1–8, https://doi.org/10.23919/EPE.2019.8915006.

[10] R. Gogoana, M.B. Pinson, M.Z. Bazant, S.E. Sarma, Internal resistance matching for parallel-connected lithium-ion cells and impacts on battery pack cycle life, J. Power Sources 252 (2014) 8–13, https://doi.org/10.1016/j.jpowsour.2013.11.101.

[11] X. Gong, R. Xiong, C.C. Mi, Study of the characteristics of battery packs in electric vehicles with parallel-connected lithium-ion battery cells, IEEE Trans. Ind. Appl. 51 (2015) 1872–1879, https://doi.org/10.1109/TIA.2014.2345951.

[12] R. Xiong, L. Li, J. Tian, Towards a smarter battery management system: a critical review on battery state of health monitoring methods, J. Power Sources 405 (2018) 18–29, https://doi.org/10.1016/j.jpowsour.2018.10.019.

[13] M. Berecibar, I. Gandiaga, I. Villarreal, N. Omar, J. Van Mierlo, P. Van Den Bossche, Critical review of state of health estimation methods of Li-ion batteries for real applications, Renew. Sust. Energ. Rev. 56 (2016) 572–587, https://doi.org/10.1016/j.rser.2015.11.042.

[14] F. Luo, H. Huang, L. Ni, T. Li, Rapid prediction of the state of health of retired power batteries based on electrochemical impedance spectroscopy, J. Energy Storage 41 (2021), 102866, https://doi.org/10.1016/j.est.2021.102866.

[15] W. Xiong, Y. Mo, C. Yan, Online state-of-health estimation for second-use lithium-ion batteries based on weighted least squares support vector machine, IEEE Access 9 (2021) 1870–1881, https://doi.org/10.1109/ACCESS.2020.3026552.

[16] E. Schaltz, D.I. Stroe, K. Norregaard, B. Johnsen, A. Christensen, Partial charging method for lithium-ion battery state-of-health estimation, in: 2019 14th Int. Conf. Ecol. Veh. Renew. Energies, EVER 2019, 2019, https://doi.org/10.1109/EVER.2019.8813645.

[17] Y. Li, H. Sheng, Y. Cheng, D.I. Stroe, R. Teodorescu, State-of-health estimation of lithium-ion batteries based on semi-supervised transfer component analysis, Appl. Energy 277 (2020), 115504, https://doi.org/10.1016/j.apenergy.2020.115504.

[18] E. Schaltz, D.I. Stroe, K. Norregaard, L.S. Ingvardsen, A. Christensen, Incremental capacity analysis applied on electric vehicles for battery state-of-health estimation, IEEE Trans. Ind. Appl. 57 (2021) 1810–1817, https://doi.org/10.1109/TIA.2021.3052454.

[19] S.B. Vilsen, D.I. Stroe, Battery state-of-health modelling by multiple linear regression, J. Clean. Prod. 290 (2021), 125700, https://doi.org/10.1016/j.jclepro.2020.125700.

[20] J. Meng, L. Cai, D.I. Stroe, J. Ma, G. Luo, R. Teodorescu, An optimized ensemble learning framework for lithium-ion battery state of health estimation in energy storage system, Energy 206 (2020), 118140, https://doi.org/10.1016/j.energy.2020.118140.

[21] L. Cai, J. Meng, D.I. Stroe, G. Luo, R. Teodorescu, An evolutionary framework for lithium-ion battery state of health estimation, J. Power Sources 412 (2019) 615–622, https://doi.org/10.1016/j.jpowsour.2018.12.001.

[22] S. Dey, Y. Shi, K. Smith, A. Colclasure, X. Li, From battery cell to electrodes: real-time estimation of charge and health of individual battery electrodes, IEEE Trans. Ind. Electron. 67 (2020) 2167–2175, https://doi.org/10.1109/TIE.2019.2907514.

[23] Q. Zhang, X. Li, C. Zhou, Y. Zou, Z. Du, M. Sun, Y. Ouyang, D. Yang, Q. Liao, State-of-health estimation of batteries in an energy storage system based on the actual operating parameters, J. Power Sources 506 (2021), 230162, https://doi.org/10.1016/j.jpowsour.2021.230162.

[24] P. Kubiak, Z. Cen, C.M. López, I. Belharouak, Calendar aging of a 250 kW/500 kWh Li-ion battery deployed for the grid storage application, J. Power Sources 372 (2017) 16–23, https://doi.org/10.1016/j.jpowsour.2017.10.063.

[25] Z. Xu, J. Wang, P.D. Lund, Y. Zhang, Co-estimating the state of charge and health of lithium batteries through combining a minimalist electrochemical model and an equivalent circuit model, Energy 240 (2022), 122815, https://doi.org/10.1016/j.energy.2021.122815.

[26] X. Sui, S. He, S.B. Vilsen, J. Meng, R. Teodorescu, D.I. Stroe, A review of non-probabilistic machine learning-based state of health estimation techniques for Lithium-ion battery, Appl. Energy 300 (2021), https://doi.org/10.1016/j.apenergy.2021.117346.

[27] S. Zhang, B. Zhai, X. Guo, K. Wang, N. Peng, X. Zhang, Synchronous estimation of state of health and remaining useful lifetime for lithium-ion battery using the incremental capacity and artificial neural networks, J. Energy Storage 26 (2019), 100951, https://doi.org/10.1016/j.est.2019.100951.

[28] Y. Li, D.I. Stroe, Y. Cheng, H. Sheng, X. Sui, R. Teodorescu, On the feature selection for battery state of health estimation based on charging–discharging profiles, J. Energy Storage 33 (2021), 102122, https://doi.org/10.1016/j.est.2020.102122.

[29] X. Lai, C. Deng, J. Li, Z. Zhu, X. Han, Y. Zheng, Rapid sorting and regrouping of retired lithium-ion battery modules for echelon utilization based on partial charging curves, IEEE Trans. Veh. Technol. 70 (2021) 1246–1254, https://doi.org/10.1109/TVT.2021.3055068.

[30] Y. Jiang, J. Jiang, C. Zhang, W. Zhang, Y. Gao, N. Li, State of health estimation of second-life LiFePO4 batteries for energy storage applications, J. Clean. Prod. 205 (2018) 754–762, https://doi.org/10.1016/j.jclepro.2018.09.149.

[31] E. Braco, I.S. Martin, A. Ursua, P. Sanchis, Incremental capacity analysis of lithium-ion second-life batteries from electric vehicles under cycling ageing, in: 2021 IEEE Int. Conf. Environ. Electr. Eng. 2021 IEEE Ind. Commer. Power Syst. Eur. (EEEIC / I&CPS Eur., IEEE, 2021, pp. 1–6, https://doi.org/10.1109/eeeic/icpseurope51590.2021.9584637.

[32] Y. Li, M. Abdel-Monem, R. Gopalakrishnan, M. Berecibar, E. Nanini-Maury, N. Omar, P. van den Bossche, J. Van Mierlo, A quick on-line state of health estimation method for Li-ion battery with incremental capacity curves processed by Gaussian filter, J. Power Sources 373 (2018) 40–53, https://doi.org/10.1016/j.jpowsour.2017.10.092.

[33] A. Barai, K. Uddin, M. Dubarry, L. Somerville, A. McGordon, P. Jennings, I. Bloom, A comparison of methodologies for the non-invasive characterisation of

commercial Li-ion cells, Prog. Energy Combust. Sci. 72 (2019) 1–31, https://doi.org/10.1016/j.pecs.2019.01.001.

[34] Y. Zhang, Y. Li, Y. Tao, J. Ye, A. Pan, X. Li, Q. Liao, Z. Wang, Performance assessment of retired EV battery modules for echelon use, Energy 193 (2020), 116555, https://doi.org/10.1016/j.energy.2019.116555.